Journal of
Ceramic Science
and Technology

J. Ceram. Sci. Technol., **13** [1] 31-38 (2022)
DOI: 10.4416/JCST2021-00014
available online at: http://www.ceramic-science.com

Influence of $ZrSiO_4$ on Honeycomb-Structured Vitrified-Bonded Ultrafine Diamond Grinding Wheels

Y. L. Ding[1, 2], W. P. Miao[*1, 2], Y. J. Zhao[1, 2, 3], H. Bao[1, 2], N. Yan[1, 2], W. Yang[2]

[1]State Key Laboratory Of Super abrasives, Zhengzhou 450001 China
[2]Zhengzhou Research Institute for Abrasives & Grinding Co. Ltd., Zhengzhou 450001 China
[3]School of Materials Science and Engineering, Zhengzhou University, Zhengzhou 450001, China
received July 20, 2021; received in revised form March 1, 2022; accepted March 6, 2022

Abstract

To improve the mechanical properties of honeycomb-structured vitrified-bonded ultrafine diamond grinding wheels and prepare high-quality silicon wafers, the effect of $ZrSiO_4$ on the performance of the grinding wheels has been systematically investigated. SEM images reveal the morphology and microstructure of grinding wheels with different amounts of $ZrSiO_4$. Thermal analysis and mechanical properties of the grinding wheel are characterized by means of TG-DSC and bending strength testing, respectively. The surface quality of ground silicon wafers is evaluated with AFM. Results demonstrate that the addition of $ZrSiO_4$ benefited the honeycomb structure and mechanical properties of the grinding wheels. When the content of $ZrSiO_4$ was 6 wt%, the grinding wheel exhibited a maximum bending strength of 42.6 MPa and wear rate of 0.46, which was 23 % higher and 18 % lower than the $ZrSiO_4$-free grinding wheel, respectively. Moreover, cracks could not be observed on surface of the silicon wafers, indicating that the surface quality of Si wafers ground by a $ZrSiO_4$-based grinding wheel was greatly improved.

Keywords: $ZrSiO_4$, vitrified-bonded, grinding wheels, Si wafers, honeycomb structure

I. Introduction

With the rapid development of computers, mobile phones and other electronic products, there is an enormous demand for small-sized integrated circuits and high-quality silicon (Si) wafers [1–3]. Hence, it is extremely important to utilize ultra-precision grinding wheels to process silicon wafers [4–6]. Among different types of grinding wheels, vitrified-bonded diamond grinding wheels demonstrate excellent self-dressing capacity, controlled porosity, ease of dressing and truing, leading to their rapid development and indicating widespread prospects [7–10]. The honeycomb-structured vitrified-bonded ultrafine diamond grinding wheel has been successfully fabricated and applied via a combination of gel casting and pore-forming agent in our previous studies [11]. However, the surface of Si wafers sometimes develops deep scratches during the grinding process. In order to continuously obtain high-quality Si wafers, the mechanical properties of honeycomb-structured vitrified-bonded ultrafine diamond grinding wheels should be improved by adding additives.

Recently, a few studies have aimed to investigate the effect of different additives and compositions on the properties of vitrified-bonded grinding wheels and ceramic materials [12]. For instance, Li *et al.* have systematically analyzed the influence of CaF_2 addition on the mechanical properties of LAS-based glass-ceramics and glass-ceramic/diamond composites [13]. The results reveal that, at a CaF_2 content of 7 wt%, the bending strength and Rockwell hardness of glass-ceramic/diamond composites improved by 27.68 % and 29.08 %, respectively. Yu *et al*. have discovered that TiO_2 addition significantly affects the bending strength, refractoriness and fluidity of vitrified bonds [14]. Baca *et al.* have demonstrated that the oxidation resistance of ZrB_2-SiC composites, sintered at 1 750 °C, is enhanced owing to the addition of Y_2O_3, resulting in desired stabilization of cubic ZrO_2 phase [15, 16].

As a promising additive, tetragonal $ZrSiO_4$ is an island-structured silicate material, rendering a low thermal expansion coefficient and excellent chemical stability [17]. Moreover, $ZrSiO_4$ decomposes into monoclinic ZrO_2 and amorphous SiO_2 during heating, where the former can diffuse within the ceramic bond and the latter can enhance the toughness of the ceramic bond owing to the volume effect [18]. Therefore, the present work mainly investigates the influence of $ZrSiO_4$ on the mechanical properties of the grinding wheels and the surface quality of ground Si wafers.

II. Materials and Methods

(1) Materials

Ultrafine diamond abrasives (~ 0 – 1 μm) were obtained from Henan Huifeng Co. Ltd., China. The pore-forming agent (PS, ~ 500 μm) was purchased from Guangzhou Meilida Co. Ltd., China. Silicon wafers, with a diameter

* Corresponding author: miao1a2b3c4@163.com

of 200 mm, were obtained from GRINM Semiconductor Materials Co. Ltd., China. N,N-methylenebis, methylacrylamide, ammonium persulfate and ammonia were obtained from Aladdin Co. Ltd., China. The ceramic bond is a kind of low-temperature bond, which was independently developed in our laboratory. Zirconium silicate grains (~ 10 μm) were obtained from Henan HongDa Co. Ltd., China.

(2) Preparation of the ceramic bond

The composition of the ceramic bond is shown in Table 1. Components were introduced in the form of lithium carbonate, alumina, silica, sodium carbonate, boric acid and potassium carbonate. The ceramic bond was prepared via sintering. Briefly, raw materials were milled for 12 h using a ball mill (with a ball-to-powder ratio of 2.5:1). Then, the mixture was melted at 1450 °C for 150 min and quenched in water. The quenched glass frits were dried, milled and eventually sieved using 325# mesh, producing ceramic bond powder.

Table 1: Chemical compositions of the vitrified bond.

Component	SiO_2	B_2O_3	Al_2O_3	Li_2O	Na_2O	K_2O
wt%	52.3	9.8	16.2	7.0	11.2	3.5

(3) Preparation of honeycomb-structured vitrified-bonded ultrafine diamond grinding wheels

The concentration of diamond abrasives of the as-fabricated grinding wheel was ~ 110 %. First, 1.0 g methylacrylamide and 0.3 g N,N- methylenebis were added into 10 mL deionized (DI) water and continuously stirred for 10 min. Then, 5.0 g diamond abrasive, 0.2 g nonionic surfactant polyvinylpyrrolidone (PVP), a certain amount of zirconium silicate and 4.0 g ceramic bond were dispersed in the above solution by stirring for 60 min. Then, 3.0 g pore-forming agent was rapidly added into the above solution. Subsequently, 0.1 g ammonium persulfate and 0.2 mL ammonia were quickly added to guarantee acrylamide gel formation. Finally, the mixture was poured into the mold and solidified, followed by drying and sintering. An optimal heating rate was formulated, as shown in Fig. 2. The green specimens were sintered in a muffle furnace in air. The free water and polymers could be removed at 150 °C and 300 °C with small holding intervals. Then, the green bodies were heated to 650 °C and held for 60 min to fuse the ceramic bond, followed by furnace-cooling to room temperature.

Sintered samples were processed into parallelepiped bars with dimensions of 50 mm × 5 mm × 6 mm for the bending strength test. To prepare the grinding wheel, samples were also processed into bulks of radians, and each bulk was 7.6 mm long, 5.0 mm thick and 4.0 mm wide. As shown in Fig. 1, the grinding wheel consisted of 28 bulks of radians. These bulks were evenly adhered to the groove at the edge of an aluminum matrix with a diameter of 209 mm. The grinding wheel, with 6 wt% zirconium silicate, was marked as the R_6-wheel. To compare results, the grinding wheel without zirconium silicate was labeled as the R_0-wheel.

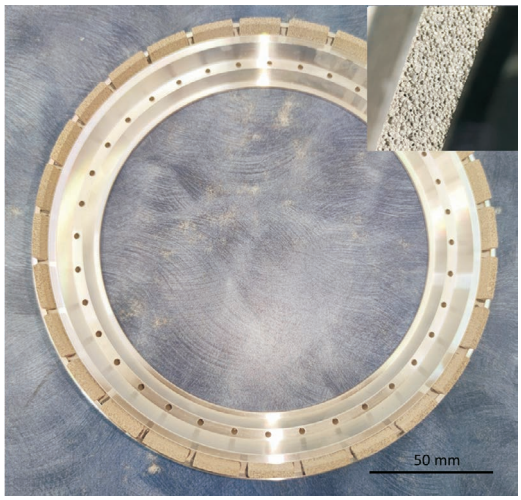

Fig. 1: Image of vitrified-bonded diamond wheels with cellular structures.

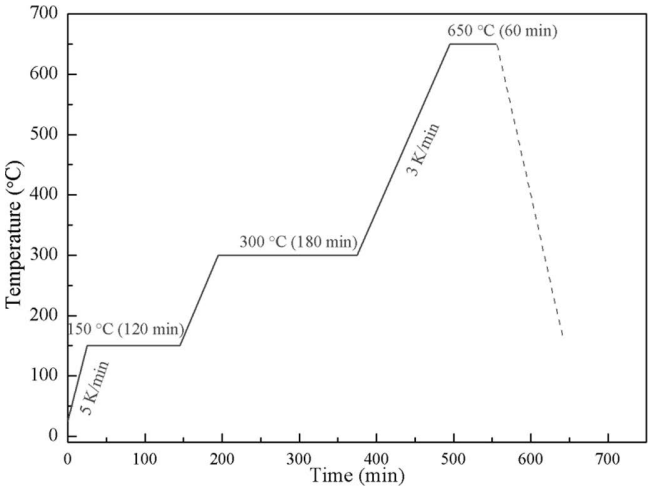

Fig. 2: The sintering schedule of vitrified-bonded ultrafine diamond wheels.

(4) Grinding of silicon wafers

The R_6-wheel or R_0-wheel was installed on an ultra-precision grinding machine (DISCO, DFG-8540) to grind Si wafers by employing a backside thinning mode. Before the grinding process, the grinding wheel was conditioned using a SiC truing plate with a mesh size of 2 000. Commercially available Si (111) wafers, with a diameter of 200 mm and thickness of 400 μm, were used for the grinding process. 100 pieces of Si wafers were ground, and each piece of Si wafer was further reduced by 30 μm using the R_6-wheel or R_0-wheel. The process parameters are summarized in Table 2.

Table 2: The parameters of the grinding process.

Grinding parameters	Wheel speed (rpm/min)	Feed rate (P1)(μm/s)	Feed rate (P2)(μm/s)	Feed rate (P3)(μm/s)	Stock removal (μm)
Super grinding	4 800	0.3	0.2	0.1	30

(5) Characterization

The honeycomb structure was analyzed using field-emission scanning electron microscope (FESEM, S-4800, Japan). Combustion characteristics of green bodies were analyzed using a thermogravimetric and differential scanning calorimeter (TG-DSC, STA-449C), where the temperature was increased at the heating rate of 10 K/min. Bulk density (ρ_b) and apparent porosity (P_a) were determined with the Archimedes immersion technique in water (Porosity analyzer, MAY-320SD). Total porosity (P_t) was calculated from the given relationship [19]:

$$P_t = 100 \times (1 - \rho_b/\rho_s)\% \quad (1)$$

where ρ_s refers to the density of grinding wheel powders, which can be obtained using the pycnometer method. Sealed porosity (P_n) is obtained from the difference between total and apparent porosity values.

An A300D-D2 blender was used to mix the experimental materials. The bending strength of the grinding wheels was measured using a (Suzhou Tophung Machine Equipment Co. Ltd., TH-8201S) bending machine. The three-point bending test was performed and calculated according to the following equation [13].

$$\sigma = \frac{3PL}{2bh^2} \quad (2)$$

where σ refers to bending strength; P denotes maximum load at breaking point; and L corresponds to span length, and b and h denote width and thickness of the sample, respectively.

III. Results and Discussion

(1) Characterization of honeycomb-structured vitrified-bonded ultrafine diamond grinding wheels

The influence of zirconium silicate ($ZrSiO_4$) content on the honeycomb structure of vitrified-bonded ultrafine diamond grinding wheels was analyzed and the results are shown in Fig. 3(a-e). In the absence of $ZrSiO_4$, the grinding wheel exhibited a complete honeycomb-like microstructure with almost closed pores (500 μm), which could effectively dissipate heat and remove debris during the grinding of Si wafers (Fig. 3a). At $ZrSiO_4$ content of 2 wt%, the honeycomb-like microstructure of grinding wheel was maintained, but the pore size was reduced to ~400 μm (Fig. 3b). Furthermore, at $ZrSiO_4$ content of 6 wt%, the pore size was reduced to 150 μm. The decrease in pore diameter increased the number of pores within a unit volume, resulting in more pore walls, contributing to the wheel strength and improving the wear resistance of grinding wheel. However, the honeycomb-like structure of the grinding wheel was damaged at a $ZrSiO_4$ content of 8 wt%, as shown in Fig. 3(e). The pores became disordered and the pore walls disappeared, hindering the grinding of Si wafers. In the absence of $ZrSiO_4$, large-sized pores were formed due to the pore-forming agent and the fluid ceramic bond. In the presence of $ZrSiO_4$, some of the $ZrSiO_4$ formed microcrystals at a certain temperature. The microcrystals will cause the accumulation of glass structure, so that the short-range order of the glass structure will be increased, promoting the stable glass phase. At high concentrations of $ZrSiO_4$, the excessive number of microcrystals inhibited the fluidity of the ceramic bond, resulting in the failure of the honeycomb structure construction, as shown in Fig. 3(e) [20].

The porosity and bending strength of the grinding wheel were also influenced by the $ZrSiO_4$ content, as presented in Fig. 4. The sealed porosity initially remained unchanged with an increase of $ZrSiO_4$ content, followed by a gradual decrease. On the other hand, the apparent porosity initially remained unchanged with increasing $ZrSiO_4$ content, followed by a gradual increase. The bending strength initially increased with increasing $ZrSiO_4$ content and attained a maximum value of 42.6 MPa at a $ZrSiO_4$ content of 6 wt%. However, the bending strength of the grinding wheel with 8 wt% $ZrSiO_4$ content was reduced to 33.2 MPa, which is consistent with microstructural features (Fig. 3). With the increase of the $ZrSiO_4$ content, the total porosity remained unchanged, but the size of the pores decreased and the number of pores increased, leading to the increase in the bending strength of the grinding wheel. At a $ZrSiO_4$ content of 8 wt%, the decrease in bending strength can be attributed to the destruction of pore walls, as shown in Fig. 3(e).

The combustion characteristics of the green bodies were assessed using a thermogravimetric and differential scanning calorimeter (TG-DSC), providing the required information for an optimal sintering protocol. As shown in Fig. 5, the curves of green bodies, with $ZrSiO_4$ content 0 and 6 wt%, were roughly the same. The volatilization of free water and combustion of polymers occurred in the temperature range of 200 to 350 °C. The exothermic peak for both samples appeared at 600 °C without any significant mass change, which can be ascribed to the fusion of the binding agent [21]. However, the peak value of curve of green bodies, with 6 wt% $ZrSiO_4$, was later than the other curve, which indicated that refractoriness of the binder was improved after the addition of $ZrSiO_4$ [22]. At 800 °C, the TG curve of $ZrSiO_4$-free and $ZrSiO_4$-containing grinding wheel was left at ~40 wt% and 46 wt%, respectively. The difference of 6 wt% is consistent with the added amount of $ZrSiO_4$.

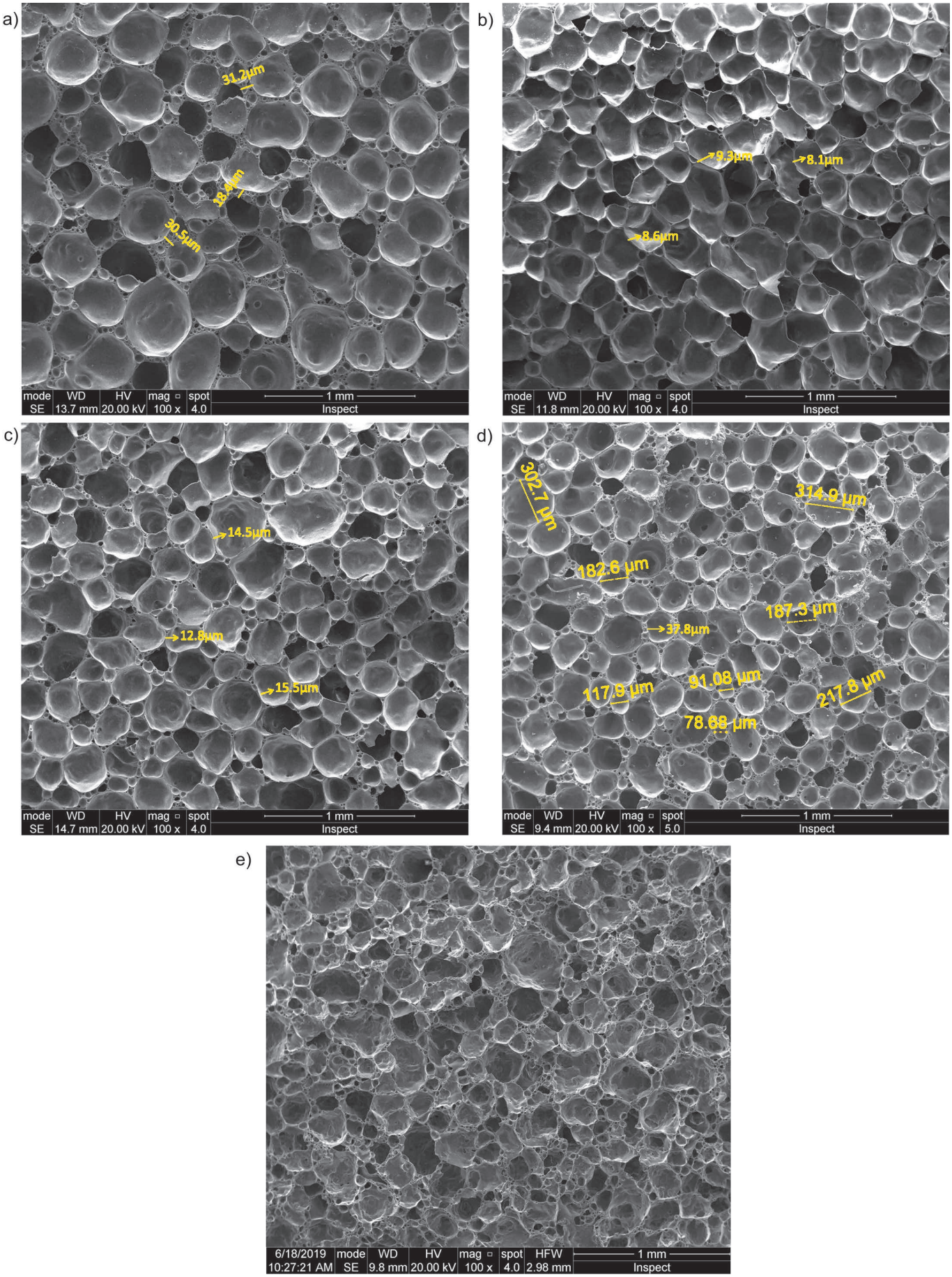

Fig. 3: SEM images of vitrified-bonded ultrafine diamond wheels with different amounts of zirconium silicate: (a): 0 %; (b): 2 %; (c): 4 %; (d): 6 %; (e): 8 %.

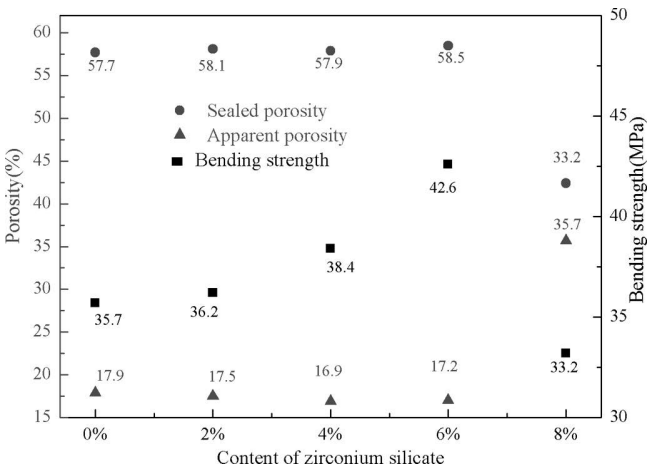

Fig. 4: Porosity and bending strength of the grinding wheel with different amounts of zirconium silicate.

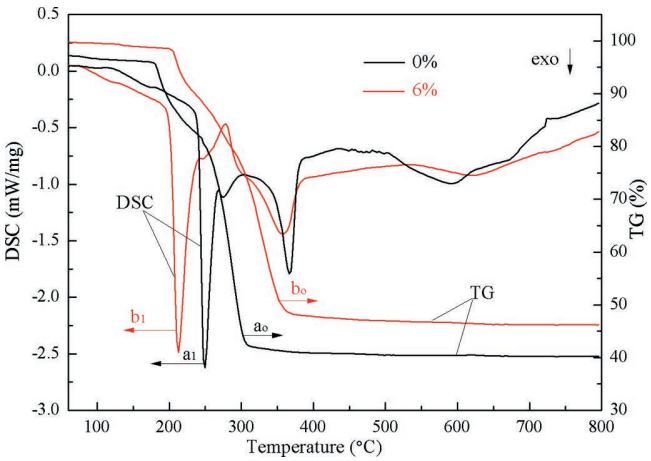

Fig. 5: TG-DSC curves of green bodies: (a_0, a_1):without $ZrSiO_4$; (b_0,b_1): with 6 wt% $ZrSiO_4$.

(2) Grinding performance

Digital photographs of Si wafers, ground by the R_6 and R_0 wheels, are shown in Fig. 6. Overall, the surface quality of Si wafers, processed by the R_6 wheel, was much better than the R_0-processed Si wafers. The microscopic photos could better contrast the differences, as shown in Figs. 6c and 6d. The surface of R_6-processed Si wafers was dark and grinding cracks could not be seen (Fig. 6c) because the specular reflection occurred under light irradiation at the smooth surface [2, 23]. However, the surface of R_0-processed Si wafers possessed dark and light areas (Fig. 6d), where dark areas were originated from the similar specular reflection (Fig. 6c) and bright areas were formed due to the remaining scratches, corresponding to the presence of a rough surface. When the light source irradiated the area, the diffuse reflection occurred and exhibited bright areas.

Furthermore, the microstructure of R_0- and R_6-processed Si wafers exhibited significant differences, as shown in Fig. 7a and 7b. For instance, R_0-processed Si wafer contained deep scratches, which have not been observed in R_6-processed Si wafer. Three-dimensional atomic force microscopy (AFM) images of Si wafers, processed by the R_0 and R_6 wheels, are presented in Fig. 8(a) and 8(b), respectively. As expected, the R_6-processed Si wafer exhibited a uniform surface without deep scratches (Fig. 8a). On the other hand, the R_0-processed Si wafer rendered an extremely poor surface, as shown in Fig. 8(b). Surface roughness of the R_6- and R_0-wheel-processed Si wafers was found to be 4.7 nm and 7.8 nm, respectively (Table 3). Through AFM analysis, the marked concave scratches in Fig. 8 were 1.6 µm in width and 91 nm in depth, as shown in Fig. 8(c). The abrasive particle size was approximately 0.75 µm, which implied that the scratches were not formed by the abrasive [24]. However, it is quite possible that the detaching grinding wheel block caused the scratching on the surface of Si wafer during the grinding process.

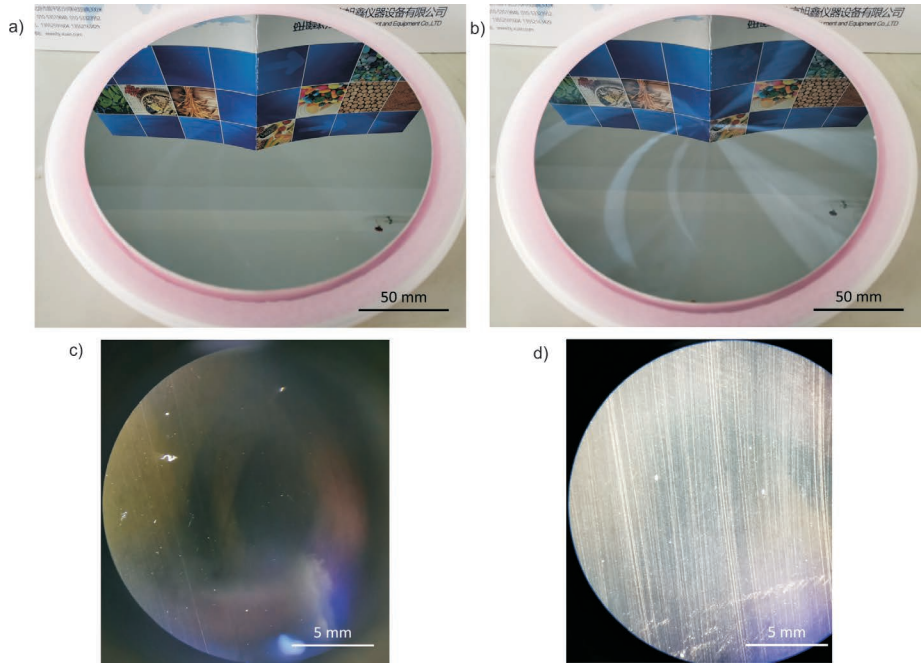

Fig. 6: Optical photographs of silicon wafers ground using the: (a) R_6-wheel; (b) R_0-wheel; Microscopic photos of silicon wafers ground using the: (c) R_6-wheel; (d) R_0-wheel.

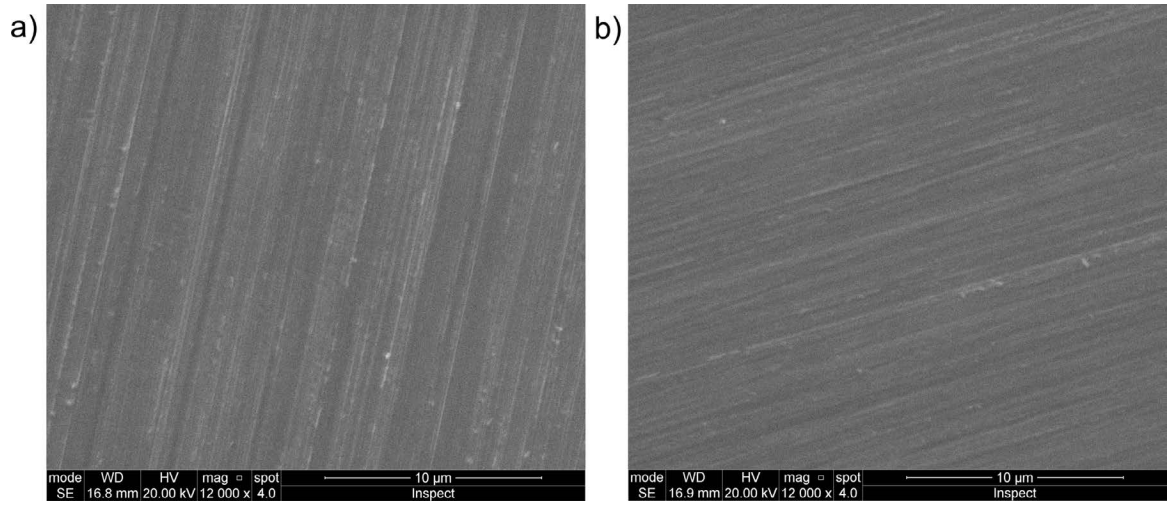

Fig. 7: SEM images of surface quality of silicon wafers ground by: (a) R_0 wheel; (b) R_6 wheel.

Table 3: The surface characteristic of ground silicon wafers

Silicon wafers	Roughness (nm)	Scratch width (µm)	Scratch depth (nm)
ground by R_0 wheel	7.8	1.6	91
ground by R_6 wheel	4.7	/	/

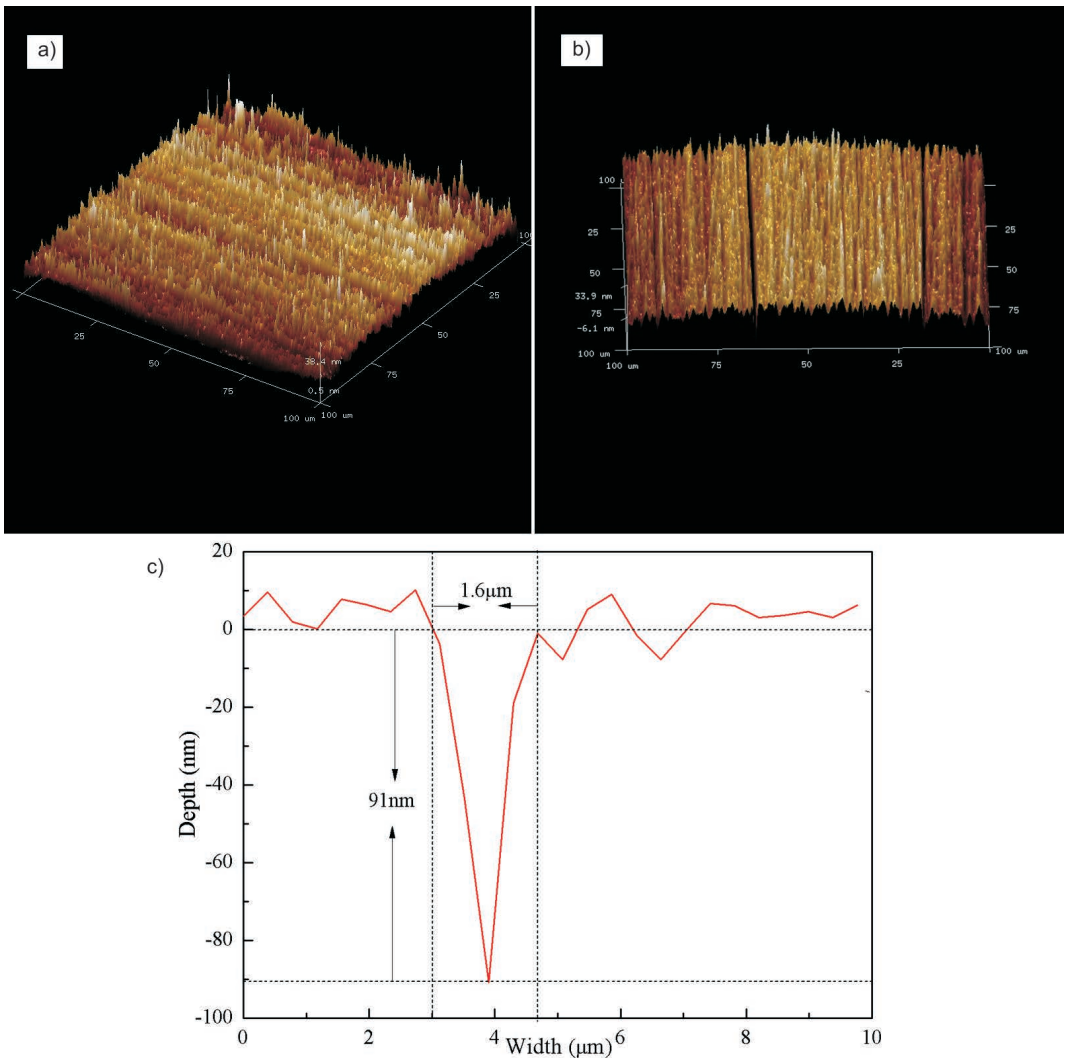

Fig. 8: AFM three-dimensional images of silicon wafers ground by: (a) R_6-wheel; (b) R_0-wheel. (c): The size of scratches on the surface of silicon wafers ground with the R_0-wheel.

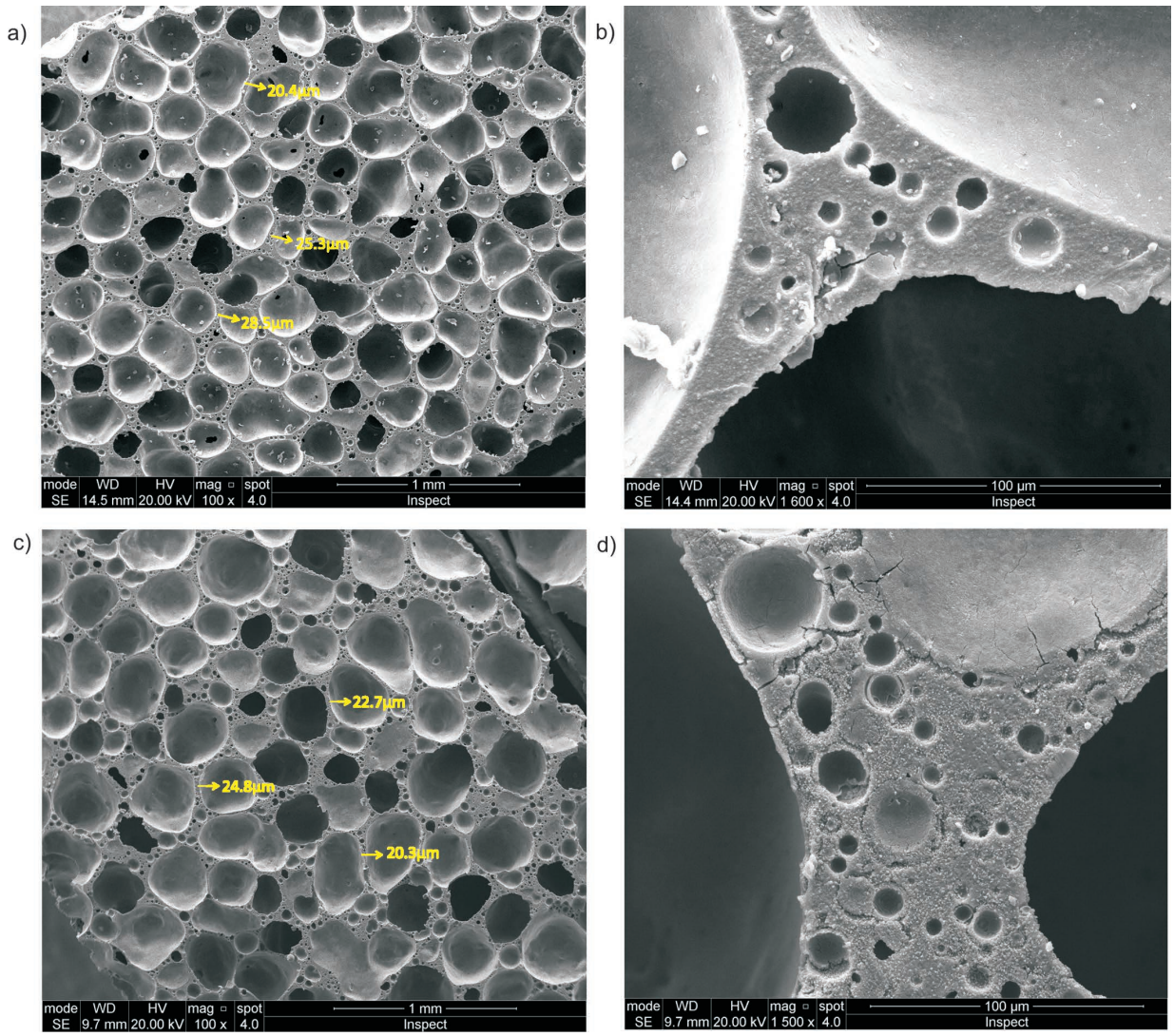

Fig. 9: SEM images of grinding surface of the: (a, b) R_0 wheel; (c, d) R_6 wheel.

The grinding mechanism of the R_0 and R_6 wheels has also been studied. During the grinding process, the honeycomb structure of grinding wheels was not damaged, and the traces of grinding could be clearly found, as shown in Figs. 9a and 9c. Clearly, the pore walls were covered with lots of tiny cracks (Fig. 9d), whereas the cracks were hardly observed in Fig. 9c. The reason may be that the strength of the R_0-wheel was low, the pore walls of grinding wheel were impacted by force and many cracks were generated during the grinding process [25]. These cracks would lead to the grinding wheel block coming off and scratching the surface of silicon wafers during the grinding process. On the other hand, the strength of R_6-wheel was improved owing to the addition of $ZrSiO_4$, cracks were not formed, and Si wafers could be efficiently processed even if the same force impacted the pore walls.

The wear rate of the grinding wheel is shown in Fig. 10. Taking the number of ground Si wafers (n) as an independent variable and grinding wheel wear (ΔH) as a dependent variable, two fitting relationships can be obtained:

$$\begin{aligned} &R_0 \text{ wheel: } \Delta H = 0.558n + 7.69,\ R2 = 0.980 \\ &R_6 \text{ wheel: } \Delta H = 0.471n + 5.16.\ R2 = 0.991 \end{aligned} \quad (3)$$

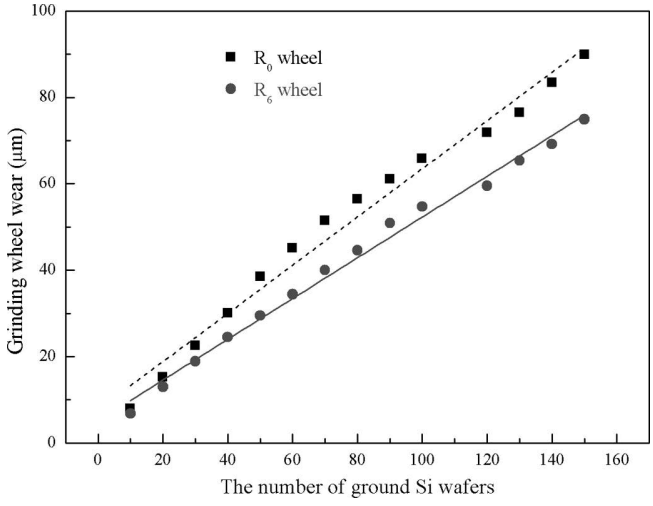

Fig. 10: Effects of the number of Si wafers on grinding wheel wear.

The dotted lines are fitted in Fig. 8. Equation (3) shows that the slopes of fitting curves represent the grinding wheel wear when grinding a piece of Si wafer. The wear rate of R_6-wheel wear is found to be 0.471 μm, which is 14.5 % lower than the R_0-wheel. Hence, the addition of

$ZrSiO_4$ reduced the pore size and enhanced the strength of the grinding wheel.

IV. Conclusions

Honeycomb-structured vitrified-bonded ultrafine diamond grinding wheels have been successfully fabricated using a combination of gel casting and pore-forming agent. Also, the influence of $ZrSiO_4$ content on pores size and bending strength of grinding wheels has been systematically studied. Briefly, $ZrSiO_4$ entered the ceramic bond structure, constituting the glass network, improving bending strength and reducing the pore size. Herein, at $ZrSiO_4$ content of 6 wt%, the grinding wheel rendered maximum bending strength of 42.6 MPa and minimal wear rate of 0.46, which was 23 % higher and 18 % lower than the $ZrSiO_4$-free grinding wheel, respectively. Overall, the surface quality of R_6-processed Si wafers had been greatly improved and cracks were not observed, which is beneficial to the subsequent chemical mechanical polishing process.

References

1 Huo, F.W., Guo, D.M., Feng, G., Kang, R.K., Wang, R.L.: A new kinematics for ultra precision grinding of conical surfaces using a rotary table and a cup wheel, *Int. J. Mach. Tool. Manu.*, **59**, 34 – 45, (2012).

2 Nakajima, K., Fujiwara, K., Pan, W., Okuda, H.: Shaped silicon-crystal wafers obtained by plastic deformation and their application to silicon-crystal lenses, *Nat. Mater.*, **4**, 47 – 50, (2005).

3 Hong, C.-S., Hong, Y.-T.: Effects of sintering temperature on structure and electrical properties of $(Na_{0.48}K_{0.473}Li_{0.04}Sr_{0.007})(Nb_{0.883}Ta_{0.05}Sb_{0.06}Ti_{0.007})O_3$ piezoelectric ceramics, *Process. Appl. Ceram.*, **15**, 79 – 86, (2021).

4 Zhang, X.H., Pei, Z.J., Fisher, G.R.: A grinding-based manufacturing method for silicon wafers: generation mechanisms of central dimples on ground wafers, *Int. J. Mach. Tool. Manu.*, **46**, 397 – 403, (2006).

5 Pei, Z.J., Fisher, G.R., Liu, J.: Grinding of silicon wafers: A review from historical perspectives, *Int. J. Mach. Tool. Manu.*, **48**, 1297 – 1307, (2008).

6 Zhou, H., Guo, M., Wang, X.: Ultraprecision grinding of silicon wafers using a newly developed diamond wheel, *Mat. Sci. Semicon. Proc.*, **68**, 238 – 244, (2017).

7 Mochalin, V.N., Shenderova, O., Ho, D., Gogotsi, Y.: The properties and applications of nanodiamonds, *Nat. Nanotechnol.*, **7**, 11 – 23, (2012).

8 Zhang, Z., Huo, F., Wu, Y., Huang, H.: Grinding of silicon wafers using an ultrafine diamond wheel of a hybrid bond material, *Int. J. Mach. Tool. Manu.*, **51**, 18 – 24, (2011).

9 Abdul, S., Yusoff, W., Baharuddin, N., Somalu, M., Muchtar, A., Osman, N.: Electrochemical performance of sol-gel derived $La_{0.6}S_{0.4}CoO_{3-\delta}$ cathode material for proton-conducting fuel cell: A comparison between simple and advanced cell fabrication techniques, *Process Appl Ceram.*, **12**, 277 – 286, (2018).

10 Kim, I.J., Gauckler, L.J.: Formation, decomposition and thermal stability of Al_2TiO_5 ceramics, *J. Ceram. Sci. Technol.*, **03**, (02), 49 – 60, (2012).

11 Miao, W., Ding, Y., Zhao, Y., Bao, H., Yan, N., Yang, W., Hui, Z., Liu, B.: Modified gel casting technique to fabricate honeycomb structured vitrified-bonded ultrafine diamond grinding wheels, *Ceram. Int.*, **46**, 4462 – 4469, (2020).

12 Ji, B., Alrayes, A.A., Zhao J., Feng Y., Shen Z.: Grinding and polishing efficiency of a novel self-glazed zirconia versus the conventional dry-pressed and sintered zirconia ceramics, *Adv. Appl. Ceram.*, **118**, 46 – 55, (2018).

13 Feng, D., Zhu, Y., Li, F., Li, Z.: Influence investigation of CaF_2 on the LAS based glass-ceramics and the glass-ceramic/diamond composites, *J. Eur. Ceram. Soc.*, **36**, 2579 – 2585, (2016).

14 Xue, S., Tianbiao, Y., Xuezhi, W., Maoqiang, X., Wanshan, W.: Effect of TiO_2 addition and high magnetic field sintering on properties of vitrified bond CBN composites, *Ceram. Int.*, **44**, 16307 – 16313, (2018).

15 Xia, P., Jiang, R., Li, Z., Zhu, Y., Sun, P.: Effect of Y_2O_3 on the properties of vitrified bond and vitrified diamond composites, *Compos Part B-Eng.*, **67**, 515 – 520, (2014).

16 Kováčová, Z., Bača, Ľ., Neubauer, E., Kitzmantel, M.: Influence of sintering temperature, SiC particle size and Y_2O_3 addition on the densification, microstructure and oxidation resistance of ZrB_2-SiC ceramics, *J. Eur. Ceram. Soc.*, **36**, 3041 – 3049, (2016).

17 Xinhong H.: Application status and development prospect of zirconium silicate in traditional ceramics, *Foshan Ceramics*, **160**, 4 – 8, (2010).

18 Keming G.: The study on sintering properties of zircon materials, *Rare Metal Mat. Eng.*, **37**, 160 – 163, (2008).

19 Zhao, C., Zhou, W., Hu, Q.H., Xu, H., Zhang, C.: Porosity measurement of granular rock samples by modified bulk density analyses with particle envelopment, *Mar. Petrol. Geol.*, **133**, 175 – 182, (2021).

20 Srivastava, V.K., Krenkel, W., D'Souza V.J.A., Mucha, H.W.: Manufacturing, analysis and modelling of porous Si-SiC ceramics derived by oxidation from C/C-Si-SiC composites, *J. Ceram. Sci. Technol.*, **02**, (02), 111 – 118, (2011).

21 Chu, Z., Jia, C., Liu, J., Ding, R., Yuan, G.: Effects of sintering time on microstructure and properties of alumina foam ceramics, *J. Ceram. Sci. Technol.*, **08**, (4), 499 – 504, (2017).

22 Rom, M., Brakhage, K.H., Barth, S., Wrobel, C., Mattfeld, P., Klocke, F.: Mathematical modeling of ceramic bond bridges in grinding wheels, *Math. Comput. Simulat.*, **147**, 220 – 236, (2018).

23 Li, K., Guo, Q., Liu, M., Zhao, Y., Shi, D.: A study on Pore-forming agent in the resin bond diamond wheel used for silicon wafer Back-grinding, *Procedia Engineering*, **36**, 322 – 328, (2012).

24 Gao, S., Huang, H., Zhu, X., Kang, R.: Surface integrity and removal mechanism of silicon wafers in chemo-mechanical grinding using a newly developed soft abrasive grinding wheel, *Mater. Sci. Semicon. Proc.*, **63**, 97 – 106, (2017).

25 Kim, K.-D., Dey, N.K., Seo, H.O., Kim, Y.D., Lim, D.C., Lee, M.: Photocatalytic decomposition of toluene by nanodiamond-supported TiO_2 prepared using atomic layer deposition, *Appl. Catal. A.*, **408**, 148 – 155, (2011).